

Bachelor-Thesis

Acousto-optical Process Control for Laser

Ablation and Laser Welding

for obtaining the degree Bachelor of Engineering (B.Eng.)

Submitted by Chen Peng

Course: Bachelor Electrical Engineering & Information Technology
Matriculation number: 27888
Date of Submission: 27.08.2019

1st Examiner: Prof. Dr. Markus Pfeil
2nd Examiner: Dr. Sven Döring

Declaration of Authenticity

I declare that this Bachelor-Thesis is my own work and I have documented all sources and materials I used in the list of references.

Location, Date

Signature

Table of Contents

1. Abstract	2
2. Introduction.....	2
3. Fundamentals.....	3
3.1 Fabry-Perot Etalon.....	3
3.2 Laser ablation.....	6
3.3 Laser welding.....	6
3.4 Beam diameter and ablation threshold.....	7
3.5 Orientation of microphone.....	8
3.6 Signal acquisition and processing.....	9
4. Experiments	10
4.1 Overview.....	10
4.2 Parameters.....	12
4.3 Precautions.....	13
4.4 Experiment Set 1: Ablation with ultrashort pulse laser at varying laser power.....	15
4.4.1 Pre-experiment	15
4.4.2 Post-experiment.....	17
4.5 Experiment Set 2: Ablation with ultrashort pulse laser at varying z-offsets.....	20
4.5.1 Pre-experiment	20
4.5.2 Post-experiment.....	23
4.6 Experiment Set 3: Welding with continuous laser at varying laser power.....	29
4.6.1 Pre-experiment	29
4.6.2 Post-experiment.....	32
5. Summary & Conclusion.....	36
6. Acknowledgments	37
7. Appendix.....	38
8. References.....	44

1. Abstract

In this thesis, an optical microphone is employed to measure airborne acoustic emissions of laser welding and ablation processes. It will be demonstrated that the measurements obtained are potentially useful in the automated calibration of the optimum focus spot of a laser beam, controlling of the laser ablation quality in a production line without modifying the workpiece, and the identification of keyhole formation (or lack thereof) during laser welding processes.

2. Introduction

In an industrial environment, the efficiency in a manufacturing process is a key component of productivity. Downtime due to anomalies in quality control, machine recalibration and destructive testing of manufactured components are several causes of lowered productivity. At BOSCH Bamberg, laser processes including ablation and welding are amongst many utilized in various forms during production. The scale of precision for process tolerances can be in the micrometer range. Conventional quality control involves destructive testing of manufactured parts, which is both labour-intensive and time-consuming. In the scope of this thesis project, a new instrument for online process control and measurement is investigated. The Eta250 Ultra is one in the series of optical microphones developed by XARION Laser Acoustics GmbH based in Vienna, Austria. The principles, usage, and limitations of this microphone in the context of laser welding and ablation process control will be discussed in this project. Theoretical concepts relevant to the completion of this thesis will be explained too.

Kacaras et al. ^[1] investigated the acoustic emission of variation in z-coordinate distance (from focusing lens to surface of workpiece) for laser ablation with similar tools employed in this thesis except for the sensor which is a piezoelectric sensor coupled to the workpiece instead of an optical microphone measuring airborne emission. Such a procedure may still hinder the automation of processes, such as the z-axis focus spot detection due to the need for physical coupling of the workpiece and the microphone. Schulze et al. ^[2] investigated the same topic, but only focusing on only acoustic emission up to 20kHz and a laser repetition rate of 1kHz. The higher frequencies of the ultrashort pulse laser machines and the relevant processes deployed at BOSCH Bamberg needs to be investigated separately. Shelyagin et al. ^[3] investigated the acoustic emission in laser welding processes, however the range of frequencies detectable is limited to below 50kHz. The experiments in this thesis aimed to look at airborne acoustic emission emitted during laser processes, with a frequency range up to 1MHz.

3. Fundamentals

Working principles of a Fabry-Perot Etalon:

The key principle of the XARION optical sensors lies in the fact that sound pressure is able to alter the optical density (and therefore the refractive index) of the medium (in this case air) that it travels through. To detect the difference in optical density, XARION optical microphones make use of a Fabry-Perot etalon (henceforth known as FPE) to set up the environment for measuring changes in laser beam intensity. Below is a picture of the microphone.



Figure 1: Sensor head of the microphone

The FPE is a parallel pair of partially reflective mirrors. Monochromatic incident light waves enter the FPE through one side. At the first reflective surface, a fraction of the amplitude is reflected while the rest is transmitted through the mirror into the FPE. At the other reflective surface, a fraction of the reflected amplitude is transmitted through the mirror and leaves the FPE while the rest is once again reflected back into it. The back-and-forth reflections continue, with each iteration seeing loss of intensity through transmission. The intensity that is reflected can be described by the Airy function.

$$I_R = 1 - \frac{1}{1+F \cdot \sin^2 \left(\frac{q}{2} \right)} \quad (1a)$$

In which ^[4]

- I_R is the reflected intensity;
- F is the Finesse coefficient

And q is the round trip phase shift, given by the equation

$$q = \frac{4\pi nd}{\lambda_0} \quad (1b)$$

In which ^[4]

- n is the optical refractive index of medium (air)
- d is distance between mirrors
- λ_0 is the wavelength of the incident light in vacuum

And the Finesse coefficient, F is given by the equation

$$F = \frac{4R}{(1-R)^2} \quad (1c)$$

In which ^[5]

- R is reflectance, the ratio of reflected power to incident power

Based on the design and assembly of the sensor, the only variable parameter in equation 1 during the operation of the sensor (equations 1a and 1b) is parameter n , which is the optical refractive index. Parameter λ_0 is a constant based on the type of laser used. The distance between the pair of mirrors in the FPE is fixed meaning no spatial displacement or mechanical deformation ^[6], hence parameter d remains a constant. The Finesse coefficient, F , is dependent on the reflectivity of the mirrors chosen, and thus parameter F can also be taken as a constant.

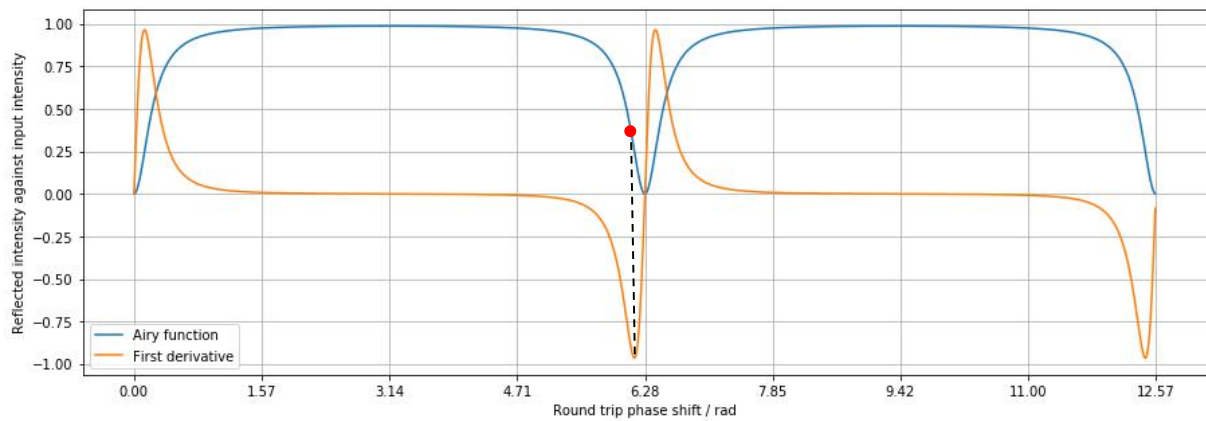


Figure 2: First derivative of the Airy function, with the red dot chosen as the nominal operating point

Figure 2 shows an example of the airy function (the ratio of reflected intensity/input intensity, against round trip phase shift), and its first derivative. From a practical point of view, only a very small range of phase shift around the point of maximum gradient magnitude on the Airy function is preferred as the nominal operation condition due to high sensitivity (to changes) and thus resolution of the incoming acoustic amplitude, as seen in Figure 2 above.

Mechanism of laser ablation:

Laser ablation is the process of material removal from the surface of a substrate by means of introducing large amounts of energy over a small, precise surface area, and over a very small duration (typically femto- up to nano- seconds) causing material to be removed by various physical means. In the context of this thesis project, we are looking at ultrashort pulse laser emitted in the order or 1-10 picoseconds onto a substrate made of steel. The entire ablation process involves the combination of several different mechanisms.

As the laser beam hits the surface of the substrate, physical events such as evaporation, sublimation and direct plasma transition occur ^[7]. Material is expelled in any case where one or more of these mechanisms are present (depending on various factors such as pulse energy, duration, substrate material etc.), and this produces disturbance in the surrounding air and hence soundwaves.

Mechanism of laser welding:

Welding is a process that employs high thermal energy to join materials, by first melting the material and then letting it cool to achieve coalescence. Laser is an ideal choice to deliver large amounts of energy over a small surface area, making it a viable tool used for welding.

Two regimes exist for laser welding, depending on the power density of laser delivered ^[8]. The first mechanism is conduction mode welding. In this regime, the thermal energy supplied causes evaporation at the surface but no keyhole is formed. Heat is transferred to the material surrounding the laser spot only through conduction to form a melt pool.

The second mechanism used to weld steel parts together is the keyhole mechanism, whereby a beam of laser hits the surface of the material, causing evaporation of said area, followed by forming a hole of metal vapour or plasma surrounded by molten metal. The vapour is mostly ejected, while residual condensed vapour together with the molten metal then cool and form a weld seam. The “keyhole” has high absorptivity of the laser energy, allowing deeper penetration of the metal surface ^[8]. The ejection of metal vapour from the surface is the major source of airborne acoustic emission.

Beam diameter and ablation threshold:

The laser beam from the ultrashort pulse laser is assumed to be a Gaussian beam, meaning the intensity of any point in the beam being a Gaussian function (refer to appendix A) with respect to the point's distance from the center of the circular cross section area of the beam. For ablation on a substrate to occur, there needs to be a minimum amount of power over a certain surface area, and this quantity is known as the ablation threshold of that material. Thus, the intensity of a laser beam on the substrate surface at any given point can be determined to be either above or below this threshold. The length of the yellow ablation threshold line which is below the beam profile is then proportional to the width (or diameter) of the ablated spot.

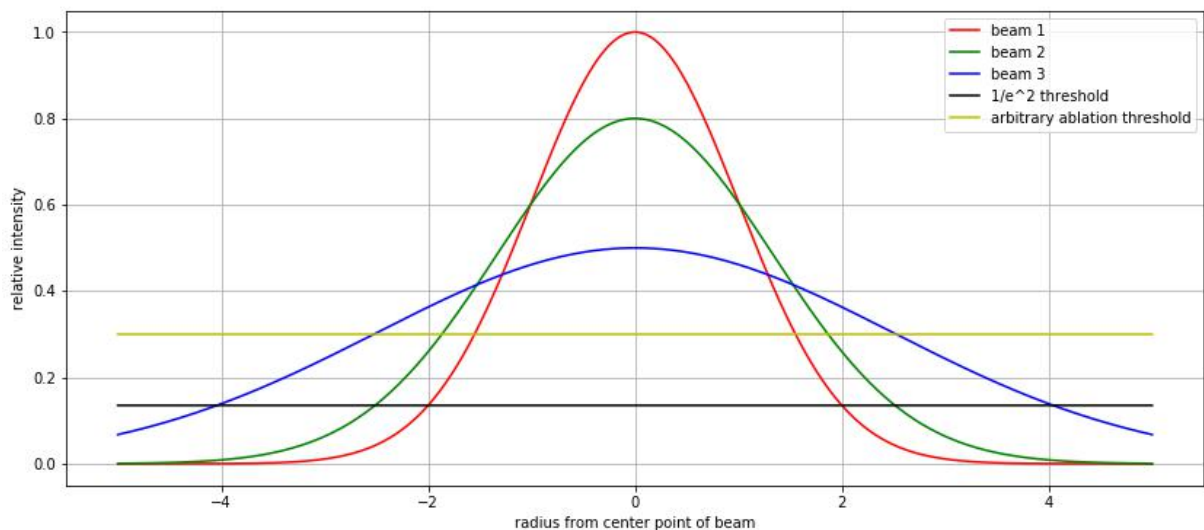


Figure 3: Some examples of laser beams with Gaussian intensity profile at the surface of the substrate

The length of the black line ($1/e^2$) which is below the beam profile is taken as the theoretical beam diameter. The different beams, 1, 2, and 3, can represent (assuming constant laser pulse frequency and energy)

1. a shift in the z-coordinate offset, with beam 1 having the smallest beam diameter (refer to appendix B) or,
2. a shift in the focal length of the focusing lens used, with beam 1 having the smallest focal length (refer to appendix B) or,
3. a combination of both the above points.

Orientation of the microphone:

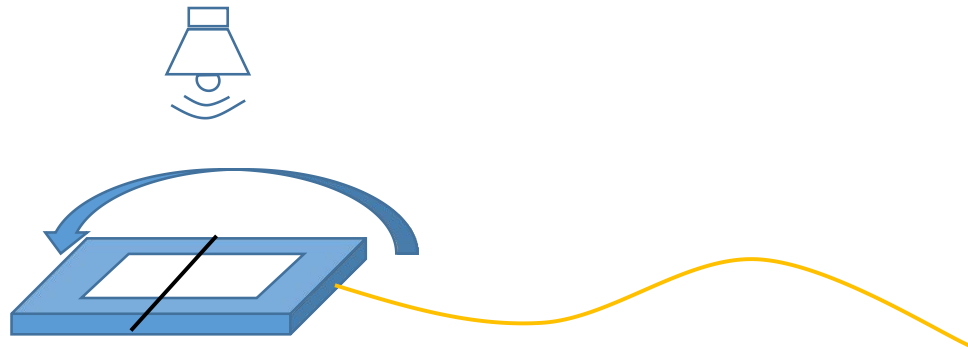


Figure 4: Illustration of rotating the sensor on its breadth, with the black line denoting the axis

To detect significant changes in the optical path length of the reflected laser, there cannot be multiple compressions and rarefactions of air in the FPE at the same time, otherwise the net effect on optical density would be minimized, resulting in greatly diminished amplitude measurement. If the sensor head is rotated in the manner shown in Figure 4, the direction of travelling soundwaves would gradually be changing from being perpendicular to the laser beam in the FPE, to being parallel. This will cause a greater section of the propagating soundwaves to modulate the laser path length at any given time (as shown in Figure 5). The end result is that the net modulation on the refractive index of air will regress toward 0, as the angle rotated approach 90°.

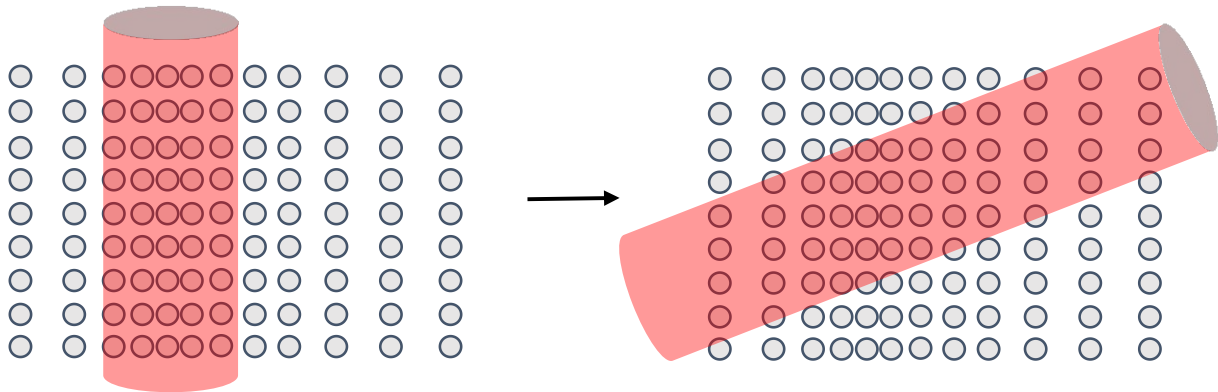


Figure 5: Difference in modulation of refractive index if the sensor is rotated as shown in Figure 4

Signal acquisition and processing:

The optical microphone itself measures changes in the optical refractive index of air and convert the measurements into an electrical signal, which is sent to the Optimizer4D computer for processing. This specialized computer contains a field-programmable gate array (FPGA) which handles real-time Short-time Fourier transform (STFT) (refer to appendix C) as the signal is read in. Changes in optical density measured by a photodiode can be treated as a time-continuous, analog quantity, it is transmitted as a voltage signal via the connecting cable first through a preamplifier device, and then to the Optimizer4D computer, which samples the voltage measurement at an adjustable sampling rate. The sample voltage is quantized by an analog-to-digital converter (ADC) (16 or 24-bit). The time-discrete, amplitude-discrete signal is then exported to be used as the primary data for further analysis.

The exported primary data can be displayed as a raw time-domain signal, or through STFT be visualized as a spectrogram with frequency, time, and amplitude axes in real-time. Due to complexity of the physics involved, it is difficult to make educated estimation of the type and nature of the acoustic emission produced by the laser processes.

4. Experiments

Overview

The following series of experiments using the XARION optical microphone attempted to provide a basis as reference for further and more in-depth experiments on laser processes, as well as to make some recommendations on upgrading current machine calibration and quality check practices based on the experimental results.

The first two sets of experiments (Set 1 and 2) are ablation processes performed with the TRUMPF TruMicro 5050 ultrashort pulse laser machine. The idea behind it is to see the established frequency of laser pulses generated by the machine, f_{mae} . The machine itself emits laser pulses at a base rate of 400 kHz. This value can be scaled down with an internal integer divider setting, meaning rates of 200 kHz, 133.33 kHz and 100 kHz etc. The microphone should be able to pick up the repetition rate of the laser pulses as ultrasonic signals.

The other set of experiments are laser welding processes performed with the TRUMPF TruDisk 1000 disk laser machine. The laser machine operates in continuous mode and deliver a constant power laser beam to the surface of a rotating cylindrical workpiece, eventually producing a continuous weld seam about its circumference. The main focus of this experiment is to capture the transition in the laser welding process, from the heat conduction regime to the keyhole (deep) welding regime.

For analysis, the key is to look for trends in the data points relative to themselves, ideally as normalized, mean, and/or aggregated values for a given set of variables. Due to the sheer number of factors (described later) that could affect the absolute read-in values by the microphone, it is not recommended to focus too much on any single absolute metric, as such a direction would hinder the repeatability and versatility of applying the microphone in an altered physical environment.

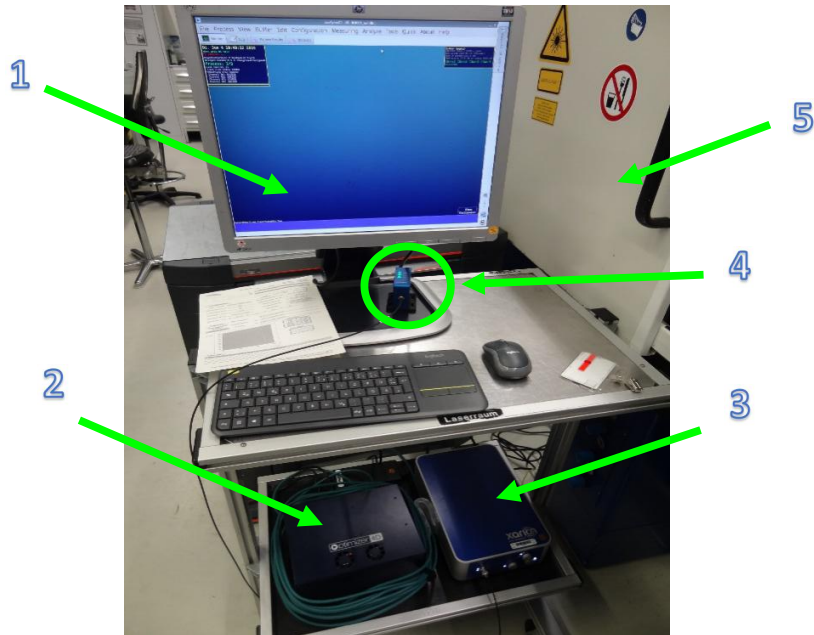


Figure 6: The optical microphone setup, with the wired microphone itself placed inside of the laser machine

The respective items in Figure 6 are as follows:

1. Monitor, connected to the Optimizer4D computer system
2. Optimizer4D computer system, containing a built in software that processes all microphone-related data
3. The optical microphone system, consisting of power supply, attenuation/gain settings, LED indicators for operation status, and BNC output port coupled to the Optimizer4D system via a pre-amplifier unit
4. Pre-amplifier unit connected to the optical microphone on one end, and the Optimizer4D system at the other
5. The door to the TRUMPF TruDisk 1000 laser welding machine.

The optical microphone will be manually triggered to start recording at the same time each experimental process is about to start, and manually stopped afterwards. The acoustic emission can be monitored in real time in the form of live STFT performed by the Analyzer4D system. The raw acoustic data that is extracted from the Optimizer4D system is in the form of binary format files (.bin) that contain an amplitude value for every discrete time unit sampled. (A one second sample at 2MHz will contain 2 million discrete time and corresponding amplitude values.) The values can be read in by a Python program for further analysis.

Parameters

Due to the intricate nature of the various components involved in this thesis, there are many parameters (adjustable constants or variables) which could affect the outcome of any single experiment. The variables investigated in the experiments that follow are just some key parameters that are of interest for further process development. In Table 1, a non-exhaustive list of parameters is listed to highlight the complexity of the experiments. A parameter is a factor that affects the outcome of an experiment. It can either be a variable or a constant depending on overall context.

Parameter	Type and nature of parameter
Optical Fiber (core diameter)	constant, property of the laser machine setup
Material of workpiece to be treated	constant, property of workpiece
Surface conditions of workpiece (microscopic/molecular)	constant (assumed), property of workpiece
Focal length (collimation lens)	variable, property of the laser machine setup
Focal length (focusing lens)	variable, property of the laser machine setup
Shielding gas flow rate	variable, independent property
Exhaust ventilation flow rate	variable, independent property
Shielding gas nozzle orientation/position	variable, independent property
Exhaust ventilation nozzle orientation/position	variable, independent property
Microphone gain/attenuation	variable, property of optical microphone
Sampling rate of microphone output signal	variable, property of Optimizer4D system
Microphone orientation	variable, independent property
Power level of welding/ablation laser	variable, property of the laser machine setup
z-coordinate offset	variable, property of the laser machine setup
Background noise	constant (assumed), independent property

Table 1: A table describing experiment parameters in within the boundaries of the thesis

Precautions

To obtain accurate and valuable results from this entire microphone measurement system, there are some pointers which should be taken into account.

1. Check for clipping of the ADC input

For any given set of experiments to be conducted, it is important to first predict (if not identify) the values of the set of parameters that would result in the highest possible amplitude among all the experiments. (For laser processes, usually the highest power/energy settings would be the logical option.) With this set of parameters, do a trial run with the microphone setup at the intended position and orientation. Observe retrospectively on the Optimizer4D graphical user interface (GUI) that the amplitude of the raw time signal recorded does not exceed the recommended range of 3×10^6 . The consequence of exceeding this recommended limit is the potential top and bottom clipping of the ADC input, which might turn an otherwise sinusoidal signal into a somewhat rectangular (or other forms) signal. Through Fourier transformation, a rectangular time signal will produce many harmonics at integer multiples of the fundamental frequency, which are undesirable, and may obscure the true form of the time signal input. In the case of the maximum amplitude exceeding the recommended range above, one can either use a connecting cable with a different attenuation value between the microphone and the pre-amplifier, or one can consider putting the microphone further away from source of the acoustic emission.

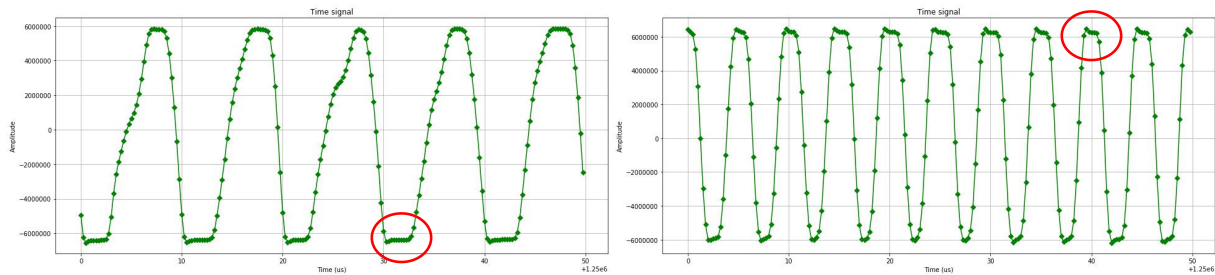


Figure 7: Examples of clipping of peak amplitude in the time signals

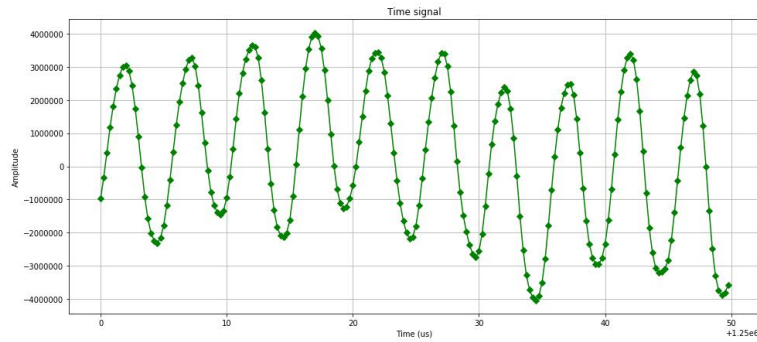


Figure 8: Example of desirable sinusoidal segments in the time signal

2. Ensure the plane of the opening of the FPE is perpendicular to the line of sight to the spot of ablation/welding

With reference to Figure 7 and 8, and the description surrounding them, it is recommended to ensure, as much as possible, that the opening of the FPE is orientated correctly for best results. The position and orientation themselves are valid parameters to be experimented on. However they are set to be constants in the experiments due to time constraints. They are also difficult to quantify as the assumption for such an experiment has to be that the surrounding physical structures and setting have to be somewhat identical for future experiments, otherwise the result may not be verifiable.

Experiment Set 1: Ablation on the surface of a workpiece with ultrashort pulse laser, step-wise variation of pulse energy (125 μ J to 12 μ J) at 3 different frequency settings

Pre-experiment

The purpose of this experiment is to have a first experience with the usage of the microphone. The ultrashort pulse laser machine is the preferred option due to its adjustable pulse frequency settings. For whichever frequency chosen it should be expected to show in the post-experiment analysis. The step-wise variation in pulse energy should appear as variation in energy analysis of the acquired data (e.g. overall root-mean-square, RMS, value of the time signal for each time signal), or simply visually distinguishable in the spectrograms generated for each process.

The following picture shows the experiment setup:

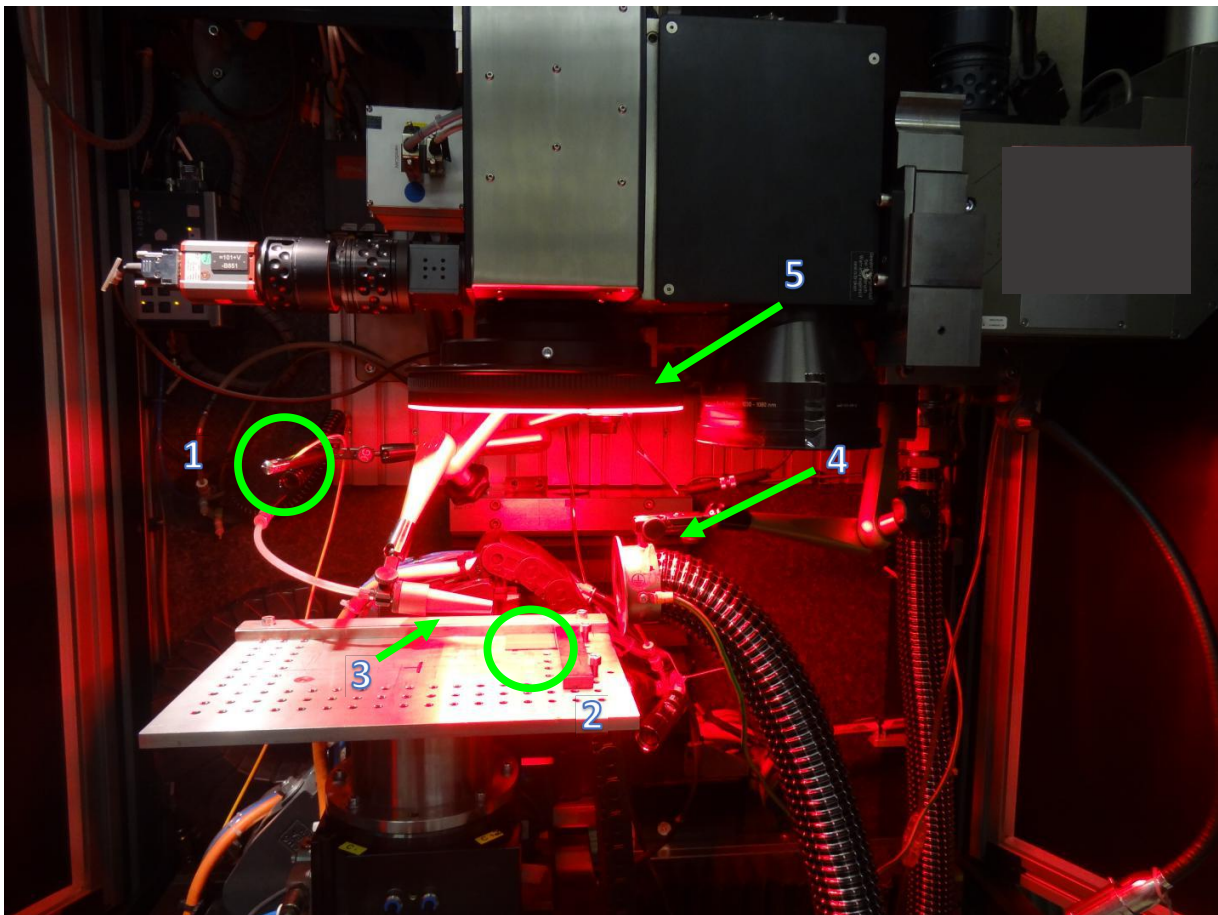


Figure 9: Setup inside the ultrashort pulse laser machine

The respective items in Figure 9 are as follows:

1. The optical microphone itself, with the plane of the etalon opening directly perpendicular to the line of sight of the ablation spot
2. The workpiece (steel plate) to be ablated
3. The nozzle providing shielding gas (nitrogen) flow
4. The opening of the exhaust ventilation
5. The focusing lens where the laser is emitted from

For each of the frequencies chosen (400 kHz, 200 kHz, 100 kHz), 10 different power levels of equal steps (100%, 90%, 80% ...) were set, with each distinct setting repeated once, giving a total of 60 ablation processes in this set of experiment. Each process is defined by a single execution of the laser program stored in the laser machine control panel and is always done on a new, untouched surface. The laser program runs as follows:

1. The supporting base plate, on which the steel plate lies, is moved to a user-defined position in space (z-coordinate constant, x- and y-coordinate can vary)
2. The laser scanner scans the surface in a straight line for a fixed distance
3. The laser scanner stops and return to the starting point of the straight line
4. Steps 2 and 3 are executed a total of 9 times
5. The program stops and the process ends

The presumptions for this experiment set are

1. The fundamental frequency should be distinctly identifiable when STFT is applied to the time signal and the result plotted on a spectrogram.
2. For the same frequency, the higher the power, the greater the overall amplitude of the sound signal and therefore greater energy of the signal.

All relevant experiment parameters (constants) are listed in the Table 2:

Focal length (focusing lens)	170mm
Distance from microphone to ablation spot	25cm
Shielding gas (nitrogen) pressure	2 bar
Ablation speed across workpiece surface	0.1ms ⁻¹
Laser properties	1030nm Yb:YAG lasers
Laser pulse duration	6ps
Focal spot size	38μm

Table 2: A list of peripheral perimeters that were set as constants

Post-experiment

The following spectrograms were obtained for their respective experimental processes.

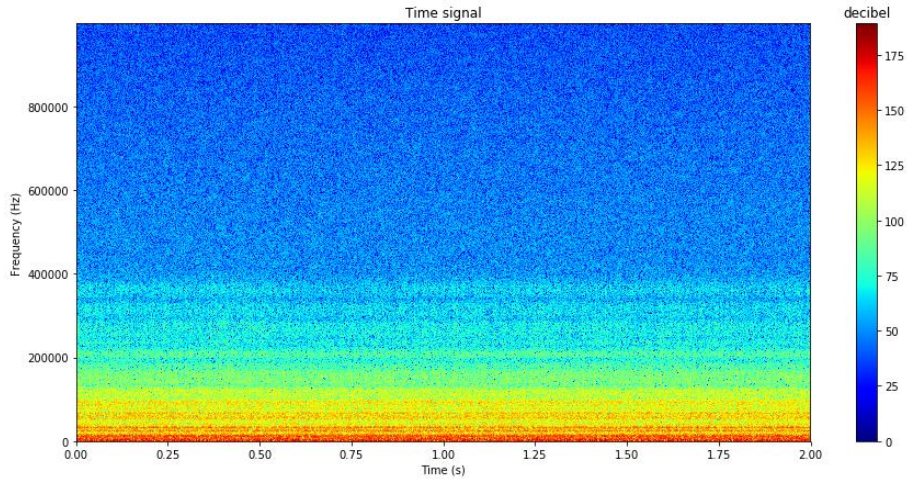


Figure 10: Spectrogram of noise signal

Figure 10 is the acoustic profile of the noise signal (background sources such as shielding gas, exhaust ventilation etc.) when the ultrashort pulse laser is not in operation, we can assume it to be a stable, homogeneous noise profile that exists throughout all other experiment processes. The likely source of this broadband noise is the shielding gas that is continuously operational during the execution of the laser program. Denoising has been attempted to visualize only the process contribution clearly (Refer to appendix D).

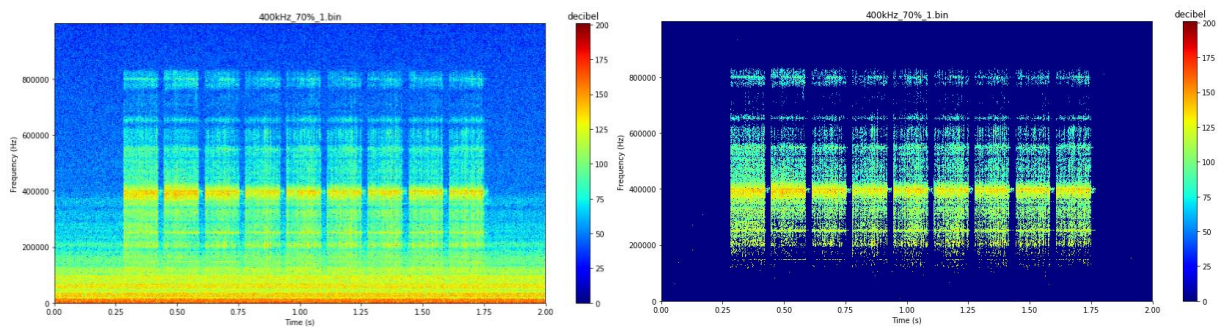


Figure 11: Ablation with 400 kHz pulses at 70% pulse energy (left: original spectrogram, right: after denoising attempt)

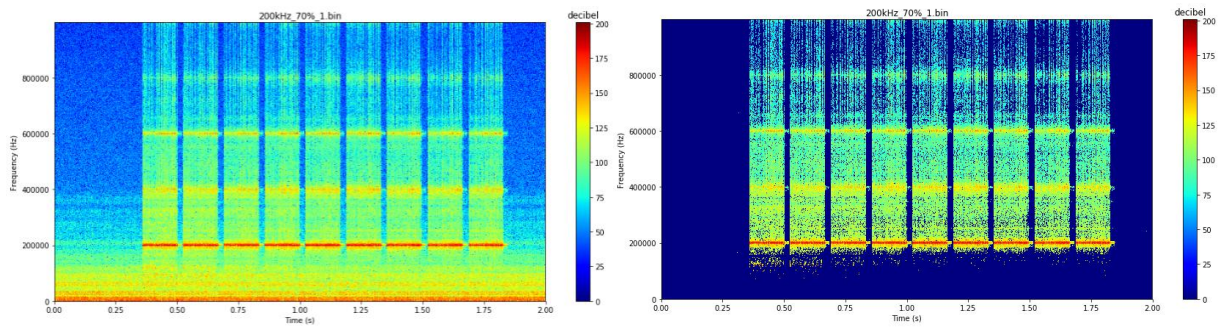


Figure 12: Ablation with 200 kHz pulses at 70% pulse energy (left: original spectrogram, right: after denoising attempt)

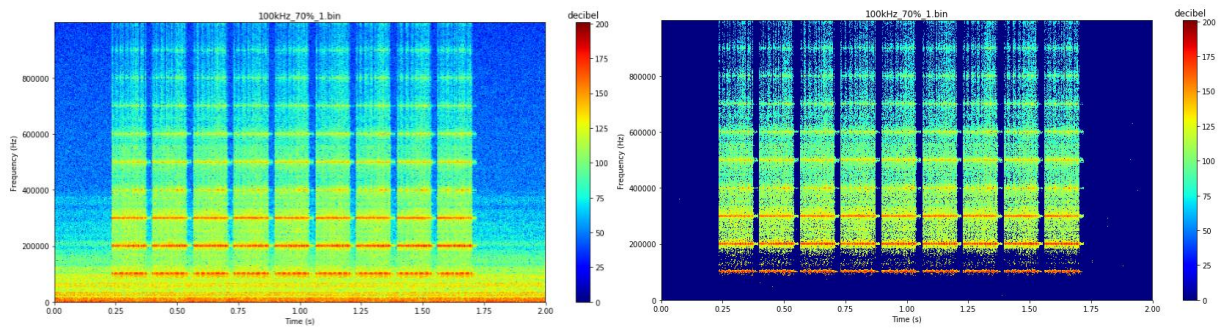


Figure 13: Ablation with 100 kHz pulses at 70% pulse energy (left: original spectrogram, right: after denoising attempt)

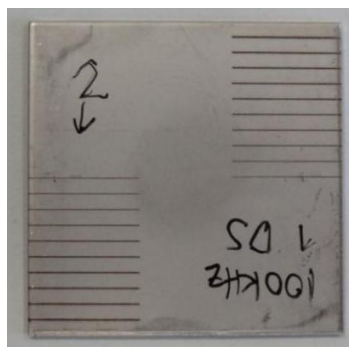


Figure 14: A steel plate showing two sequences of ablated lines, done with 100kHz, laser from 125 μ pulse energy (thickest) to 12 μ energy (thinnest)

Figure 14 shows a physical sample obtained after two processes.

Figure 11, 12, and 13 shows the spectrogram of a single process using 400kHz, 200kHz, and 100kHz laser pulses respectively. The horizontal axis denotes time, the vertical axis denotes frequency, and the colour denotes the logarithmic amplitude of each time-frequency bin, with blue being the lowest and red being the highest. It is evident that the fundamental frequencies of the laser pulses in each case are easily identifiable. However it is important to note here, that the signals from which these spectrograms are calculated are problematic.

As mentioned in the “Precautions” section, the presence of local peaks around the integer multiples of the fundamental frequencies can be a result of the nature of the Fourier transformation, because the raw time signal in each window of transformation is distorted due to clipping. It results in a periodic signal which looks like it consists of rectangular waves, albeit still based on the fundamental frequency set by the laser program. It is perhaps reasonable to expect that higher (may or may not be harmonic) frequencies in the acoustic profiles are inherent features of the ultrashort pulse ablation processes, because the source of the emission is not perfectly sinusoidal. However, distortions due to clipping still obscure the true amplitudes and frequencies of sinusoidal components that make up the actual time signal, rendering any further analysis and comparisons of the data erroneous. The repeated set of processes serve as a confirmation that the acoustic profiles obtained were indeed consistent and not anomalous.

The spectrograms validate the first presumption mentioned above, indicating clearly the fundamental frequency of the laser pulses deployed in each case with acceptable accuracy. The second presumption unfortunately cannot be examined due to clipping of the time signals. Computed comparisons of the energy levels of the acoustic emissions are not valid due to the reason mentioned above, while visually, the spectrograms do differ noticeably at lower power levels, but are expectedly less distinguishable at higher power levels (refer to Appendix E), as clipping of the time signal occur at a higher rate.

Experiment Set 2: Ablation (straight lines) with ultrashort pulse laser, step-wise variation of z-coordinate offset, 0 μ m to \pm 2150 μ m

Pre-experiment

The purpose of this experiment is to investigate any possible correlations between the z-offset from the optimum focus point and the acoustic signals received by the microphone. The z-offset is the perpendicular (z-coordinate, or vertical, refer to Figure 15) distance from the optimum focus spot. The future applications of such a successful characterization include automating the process of locating the ideal focus spot and identifying unexpected deviations from the ideal focus spot during production.

The following picture shows the experiment setup:

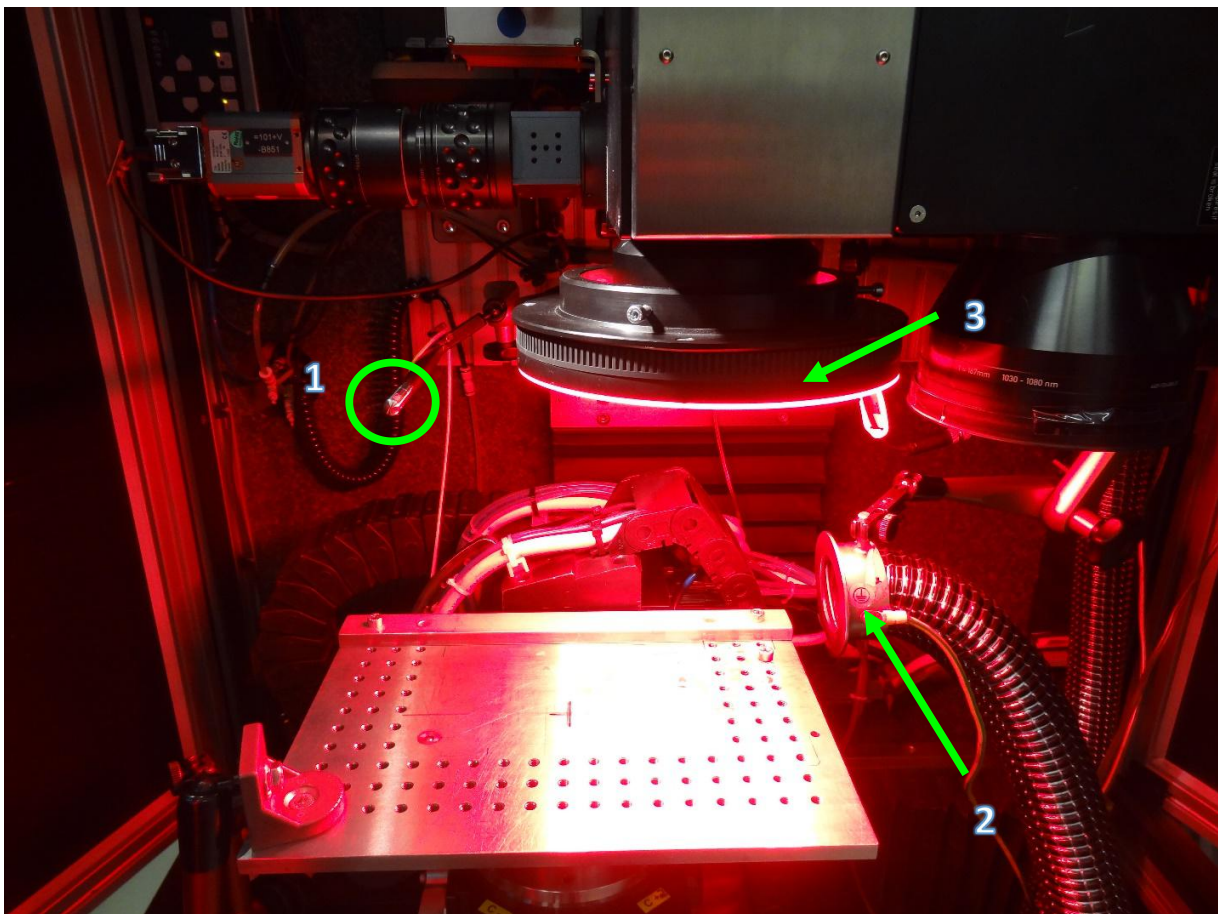


Figure 15: Setup inside the ultrashort pulse laser machine

The respective items in Figure 15 are as follows:

1. The optical microphone itself, with the plane of the etalon opening directly perpendicular to the line of sight of the ablation spot
2. The opening of the exhaust ventilation
3. The focusing lens where the laser is emitted from

Two subsets of experiments were conducted with different focusing lens, one of 170mm focal length, and the other of 80mm. With each focal length, 3 different pulse frequencies: 200kHz, 133kHz, and 100kHz (400kHz base frequency with integer dividers) were set, each for a sequence of z-coordinate offset values (see Table 3). Each sequence is repeated two times, to give 3 samples for every distinct combination of variables.

The laser program runs as follows:

1. The supporting base plate, on which the steel plate lies, is moved to a user-defined position in space (z-coordinate constant, x- and y-coordinate can vary)
2. The laser scanner scans the surface in a straight line for a fixed distance
3. The laser scanner stops and return to the starting point of the straight line
4. Steps 2 and 3 are executed a total of 3 times
5. The position of the base plate is shifted to expose a new surface with the next z-coordinate offset value included
6. Steps 2 – 5 are repeated until a sequence of 13 (positive or negative, set before start of program) z-coordinate offset values are completed.

In total, there would be 18 executions of the laser program (3 pulse frequencies * 2 z-coordinate directions * 3 samples per combination), and 234 iterations of laser pulses (18 executions * 13 offset values).

Offset from ideal focus spot (smallest area) in μm												
± 0	± 100	± 200	± 300	± 400	± 500	± 650	± 900	± 1150	± 1400	± 1650	± 1900	± 2150

Table 3: A table of z-coordinate offset values used

All relevant experiment parameters (constants) are listed in the Table 4 below:

Focal length (focusing lens)	170mm/80mm
Distance from microphone to ablation spot	24cm
Shielding gas (nitrogen) pressure	No shielding gas
Ablation speed across workpiece surface	1.0ms ⁻¹
Laser properties	1030nm Yb:YAG lasers
Laser pulse duration	6ps
Thickness of steel plate ablated	1.25mm
Focal spot size	38μm / 18μm

Table 4: A list of peripheral perimeters that were set as constants

The z-coordinate for which the 0μm offset is designated was experimentally determined before the start of the experiment. It is found by ablating a steel plate of 1.25mm thickness at various z-coordinate values and examining the results under a microscope to look for the ablated line with the thinnest width (beam diameter). It is worth pointing out that this process of locating the optimum z-coordinate value is exactly one of the reasons for investigating the application of the optical microphone for this case.

Post-experiment

Examples of physical results of the experiments are as follows:

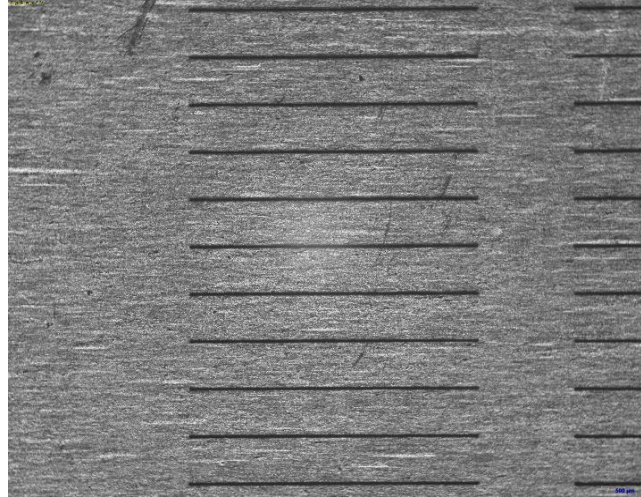


Figure 16: A whole series of line ablation done sequentially with step-wise varying z-offset. A column of these lines represent one execution of the laser program

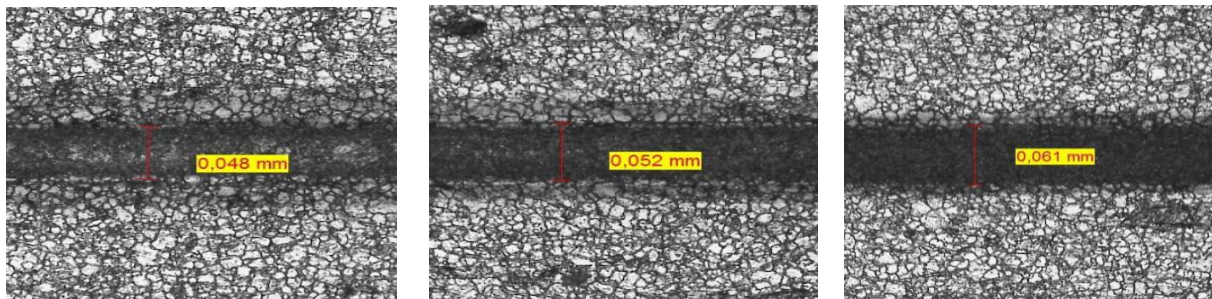


Figure 17: 170mm focal length, 200kHz laser pulse frequency, from left to right: 0μm, +500μm, +2150μm z-offset

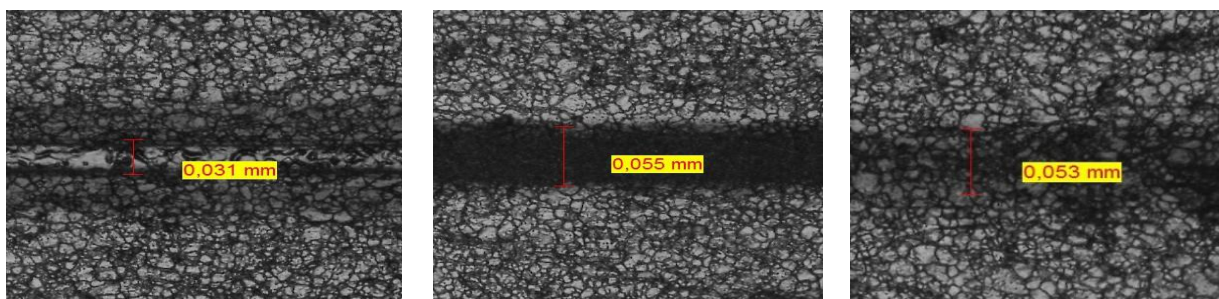


Figure 18: 80mm focal length, 200kHz laser pulse frequency, from left to right: 0μm, +500μm, +2150μm

The correlation found between the z-coordinate offset values and the respective acoustic profiles manifests itself most prominently and consistently as the root-mean-square (RMS) value of the raw time signal of the respective pulses, showing a relative maximum of the RMS value at $0\mu\text{m}$ z-coordinate (smallest focus spot size). In Figure 19 and 20 below, each point in the graph represents a mean value of the 3 iterations of laser pulses with identical parameters. The 3 different colours red, green, and blue represents experiments done with laser pulse frequency of 200kHz (400kHz/2), 133kHz (400kHz/3), and 100kHz (400kHz/4) respectively. It is evident that the points start at a maximum (normalized) value of 1.0 at the center of $0\mu\text{m}$ offset and decreases in both directions as the magnitude of z-offset increases. However, the rate of decrease and overall shape of the graphs are inconsistent and therefore not suitable to be fitted to any well-known distributions at this juncture, but this may be resolved based on the reasoning provided later.

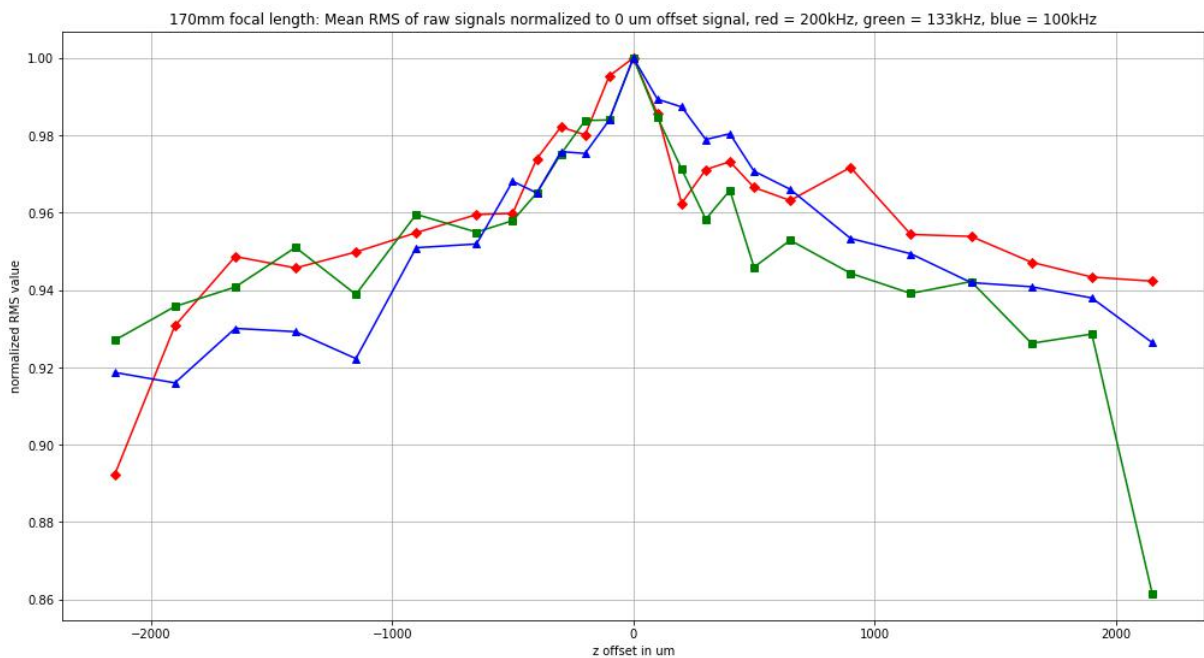


Figure 19: Graph showing normalized mean RMS values of time signals against z-coordinate offset for the subset of experiments done with the 170mm focusing lens

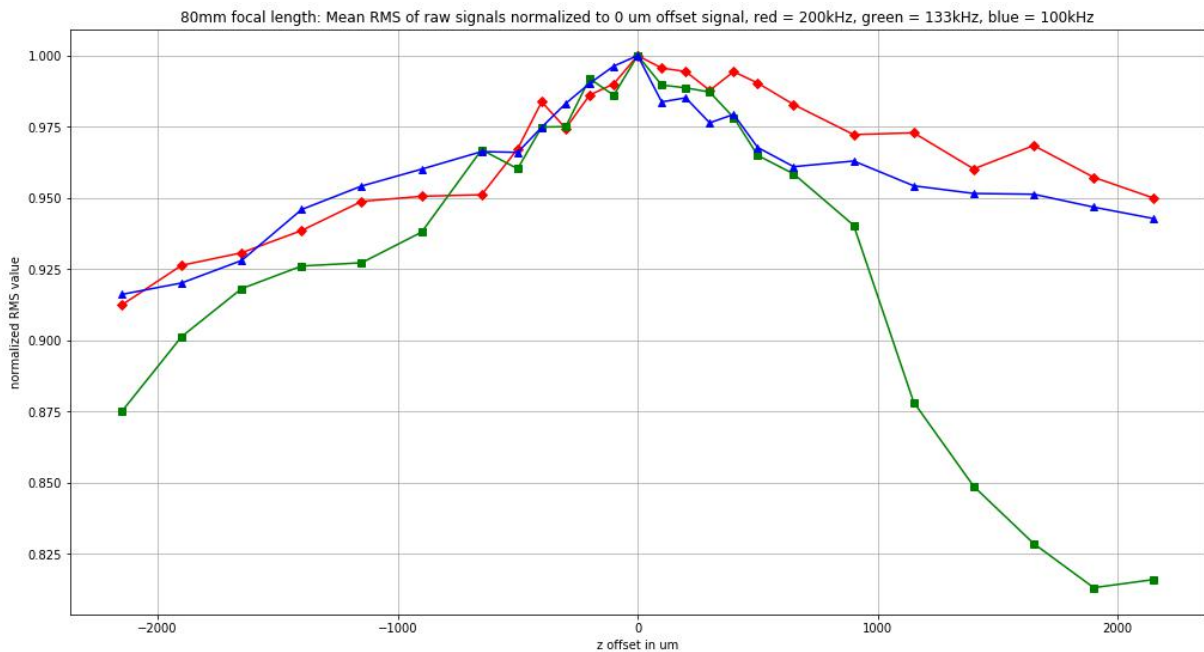


Figure 20: Graph showing normalized mean RMS values of time signals against z-coordinate offset for the subset of experiments done with the 80mm focusing lens

The execution of a laser program is timed manually to coincide with the start of a recording with the microphone. There are also minute yet relatively non-negligible differences in the duration between each iteration of laser pulses. These two factors result in great difficulty doing time-precise comparisons between the acoustic emissions of different iterations. As a compromise, every iteration is isolated from the source recording with significant duration of noise before and after the actual ablation process (see Figure 21).

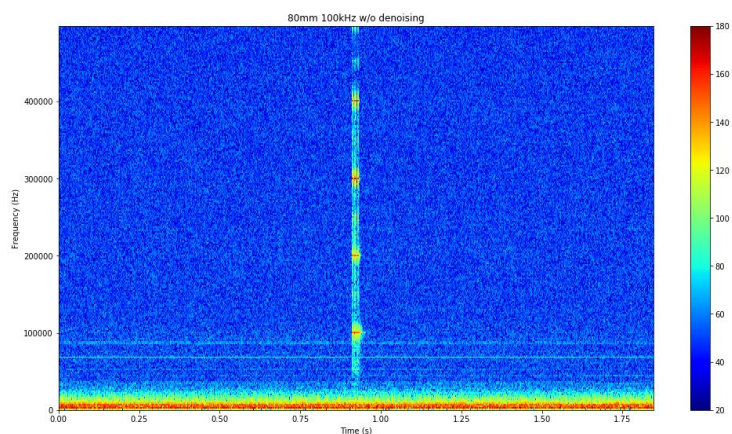


Figure 21: Spectrogram of the entirety of the signal containing the 0 μ m offset process at 80mm focal length and 100kHz laser pulses

When the RMS of each ablation signal is calculated, it includes all the contribution from the irrelevant noise as locating the precise start and end of each ablation signal is inefficient. Proportionally, the contribution to the RMS value of the actual ablation process is smaller if the total duration of the noise contained in the calculation is longer. Variations in the actual noise profile in the experiments could then have a larger effect on the RMS value seen above. Despite this factor, the analysis still produced a distinct feature mentioned above. Thus there is reason to believe that for future applications, if there is a trigger signal from the laser machine to precisely synchronize the start of the laser program and the microphone recording, RMS values can be calculated for only the exact duration of the ablation process to see differences in the signals that could be more pronounced, and the overall graphs will contain less fluctuations. This result could be the basis for further investigation into this characteristic, to confirm the applicability of using the RMS values of a sequence of line ablations done with stepwise z-coordinates variations, to determine the optimum z-coordinate without needing manual efforts using the microscope.

An attempt at denoising was also made for spectrograms generated in this set of experiments.

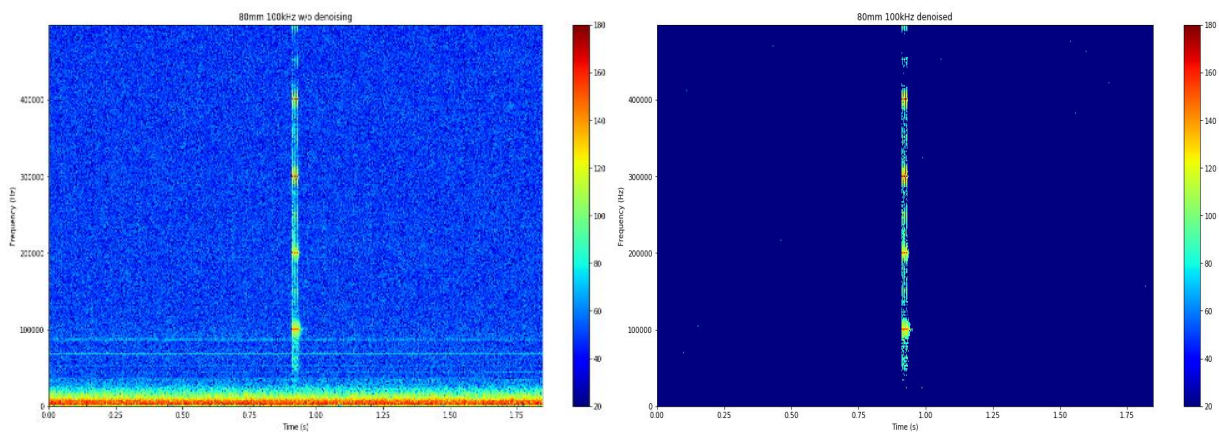


Figure 22: Left: spectrogram before denoising. Right: spectrogram after denoising

After denoising, the power spectral density (PSD) was calculated for each spectrogram. It is the summation of all the squared amplitude for each discrete time-frequency bin. The normalized values (against the z-offset = 0 μ m process data) are plotted in Figure 23 and 24.

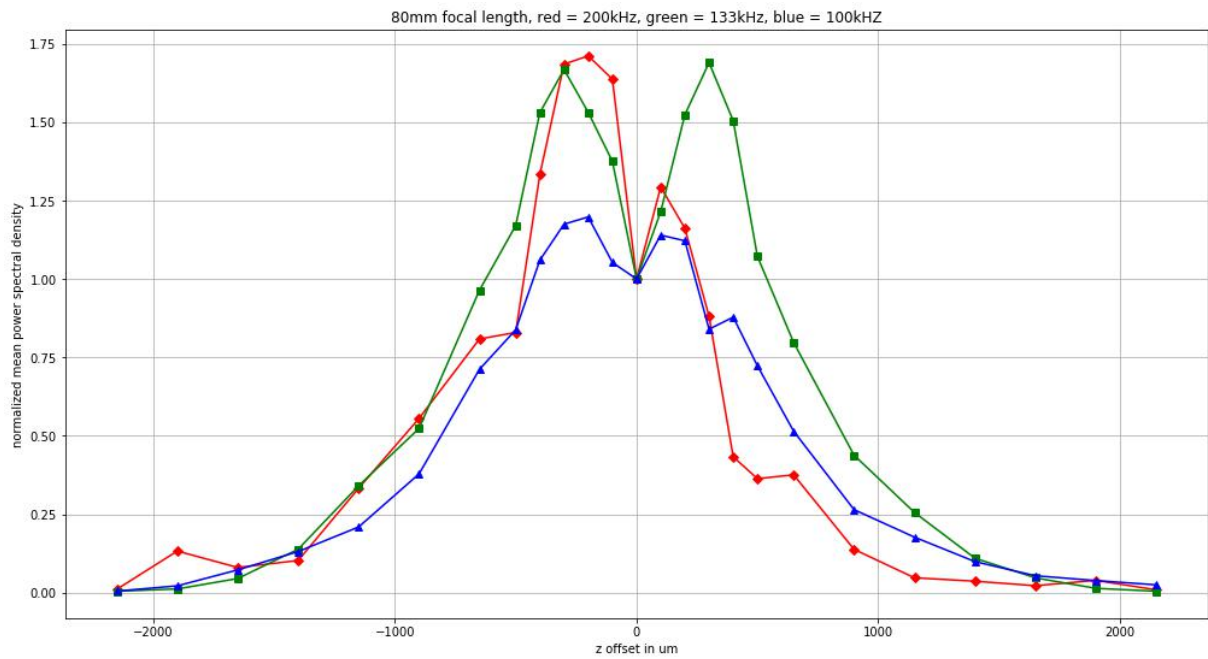


Figure 23: Normalized mean of PSD for each z-offset process done with the 80mm focusing lens

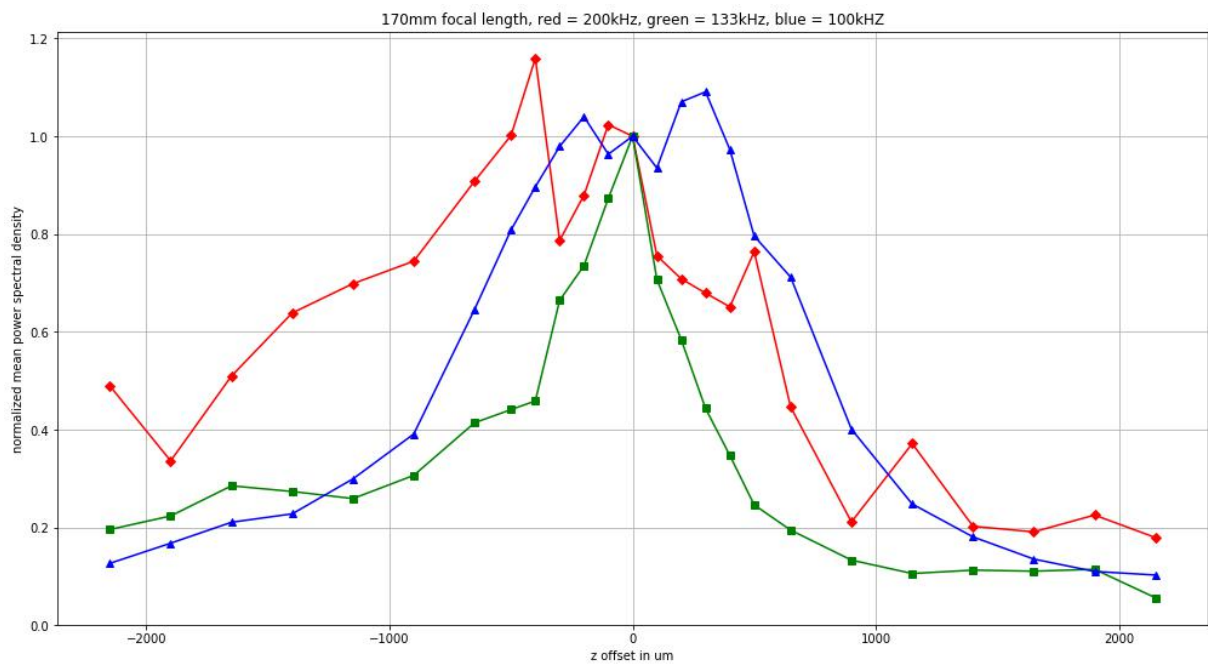


Figure 24: normalized mean of PSD for each z-offset process done with the 170mm focusing lens

From Figure 23, it is evident that the PSD values for ablation processes done with the 80mm lens are at a local minimum at $z=0\mu\text{m}$ offset. The PSD values then rose when the magnitude of the offset was increased for a few steps before then dropping continuously as the magnitude of the offset continuously increased. However, this trend manifested inconsistently, if at all for ablation processes done with the 170mm focusing lens. This is perhaps reasonable as the intensity of the laser beam vary at a different rate given the same sequence of z-coordinate offsets due to the difference in focal length. The 80mm focal length is expected to have a shorter Rayleigh length and a smaller beam waist too.

Kacaras et al. ^[1] have done a similar experiment which seem to suggest that the shape seen in Figure 23 could be a point of interest for further investigation, as it is suspected that the overall acoustic emission of an ablation process depends on both the ablation width and depth. The width and the depth are ultimately dependent on a variety of parameters such as laser power, number of laser scans, the scanning speed, the ablation threshold of the material involved, and the focal length of the lens used. All these parameters determine the final outlook of the physical events happening on the surface of the ablated material. Any success in confirming the above-mentioned trend in PSD values with regards to the z-offset value could, even if for only certain sets of experiment parameters, be very helpful in the accurate, automated determination of the optimum focus spot.

There are also different ways of analyzing the data collected. RMS and PSD are just two of the characteristics examined, with many more remained to be explored. The important idea is that the acoustic data generated from physical processes can be analyzed live. The monitoring of production processes in this manner can also be scaled up given enough computing power, since it is flexible and less labour intensive.

Experiment Set 3: Welding on the surface of a workpiece with continuous-mode laser, step-wise variation of laser power (280W to 450W)

Pre-experiment

The purpose of this set of experiments is to investigate the influence of laser power on the acoustic emission in laser welding.

The following picture shows the experiment setup:

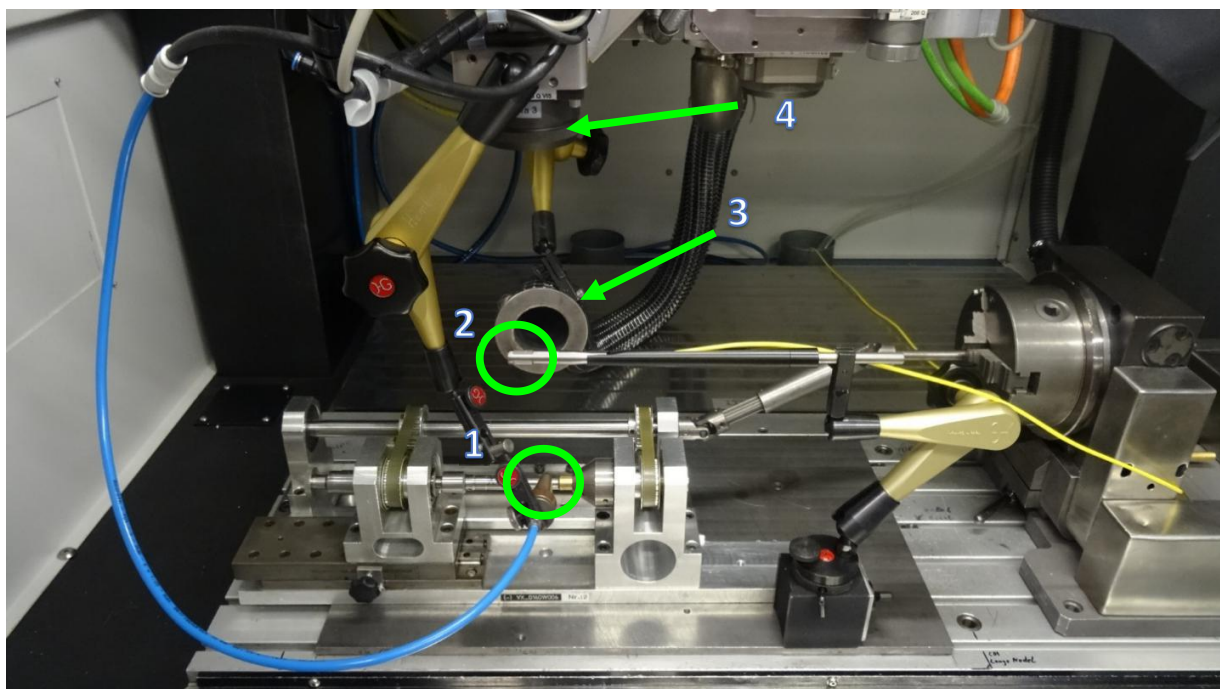


Figure 25: Welding setup inside the continuous-mode laser machine

The respective items in Figure 25 are as follows:

1. The shielding gas nozzle pointing directly at the welding spot on the cylindrical workpiece
2. The optical microphone, with the plane of the etalon opening directly perpendicular to the line of sight to the ablation spot
3. The opening of the exhaust ventilation
4. Focusing lens where the laser beam is emitted from



Figure 26: The display on the laser control panel, with the center of the crosshair pointing directly at the welding point

The range of power chosen was the result of some preliminary tests where large steps of power levels were used to narrow down the range of interest. The specific power levels chosen are as follows

280W	290W	300W	310W	315W	320W	325W	330W	335W	340W	345W	350W	355W
360W	365W	370W	375W	380W	390W	400W	410W	420W	430W	440W	450W	

Table 5: Table of power levels investigated

The shape of the laser pulse for each welding process is always a trapezium as depicted below. The laser program starts at a base 30W and rises to the user-defined power level within a fixed duration of 30ms, stays at that level until 1100ms and then decreases to 30W within 60ms. This duration chosen corresponded one round trip of the laser around the circumference of the workpiece.

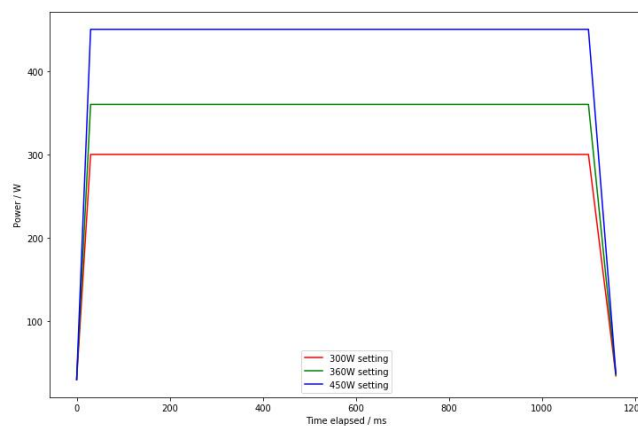


Figure 27: Examples of the laser pulse shape for 3 different power levels

The process consisted of the execution of the laser program above while the cylindrical workpiece is being rotated one round along its length axis. Each process with a distinct power level is repeated to give a total of 50 processes. The process however does not actually involve the coalescence of material from two separate workpiece, instead it is simplified to have the continuous laser effect the same workpiece, which is sufficient to produce the welding mechanisms.

All relevant peripheral parameters (constants) are listed below:

Optical fibre core diameter	100 μ m
Focal length (collimation lens)	200mm
Focal length (focusing lens)	300mm
Distance from microphone to ablation spot	24cm
Shielding gas (nitrogen) flow rate	600 ℓ / h
Welding speed across workpiece surface	1.5ms ⁻¹
Laser properties	1030nm Yb:YAG lasers
Diameter of workpiece	7.5mm

Table 6: A list of peripheral parameters that were set as constants

Post-experiment

Compared to the acoustic profiles of purely heat conduction regime welding processes, broader band and higher amplitude spectra are speculated to occur in the time slices which keyholes form. The following sets of graphics show the corresponding spectrograms of the acoustic emission and the corresponding cross sections of the weld seam which is treated in that process.

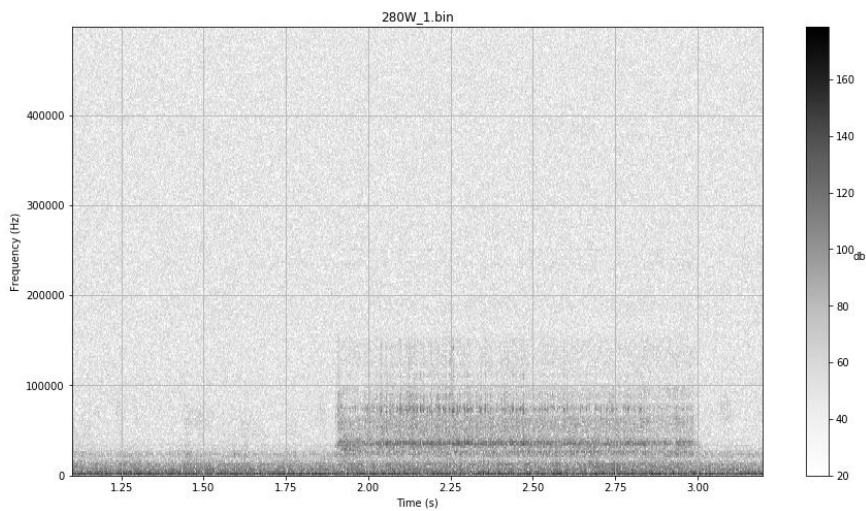


Figure 28: Spectrogram for the acoustic emission of a 280W laser process in the heat conduction regime



Figure 29: 3 weld seams from different cross sections of a weld seam at 280W laser process

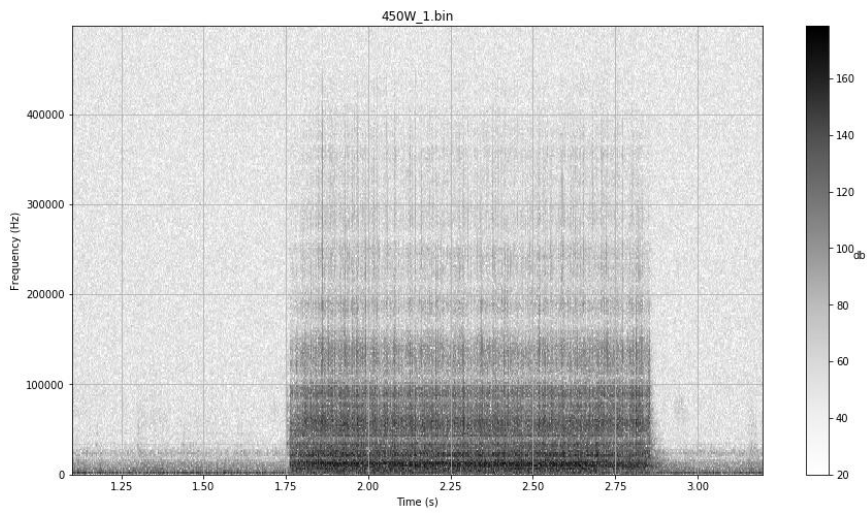


Figure 30: Spectrogram for the acoustic emission of a 450W laser process in the keyhole/deep welding regime

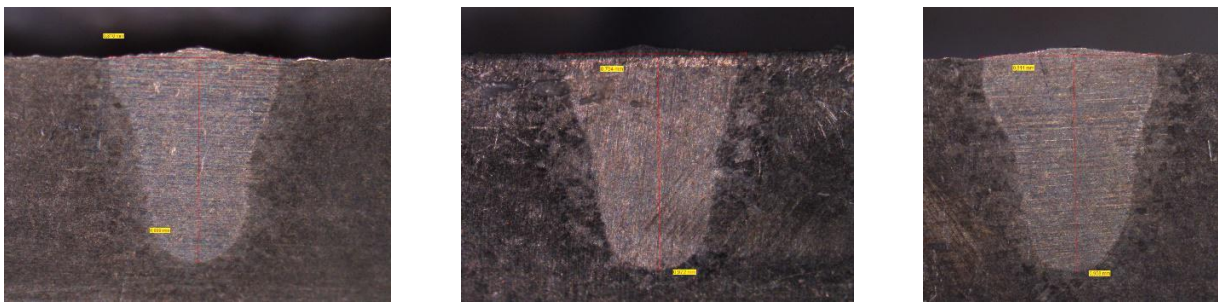


Figure 31: 3 weld seams from different cross sections of a workpiece treated in a 450W laser process

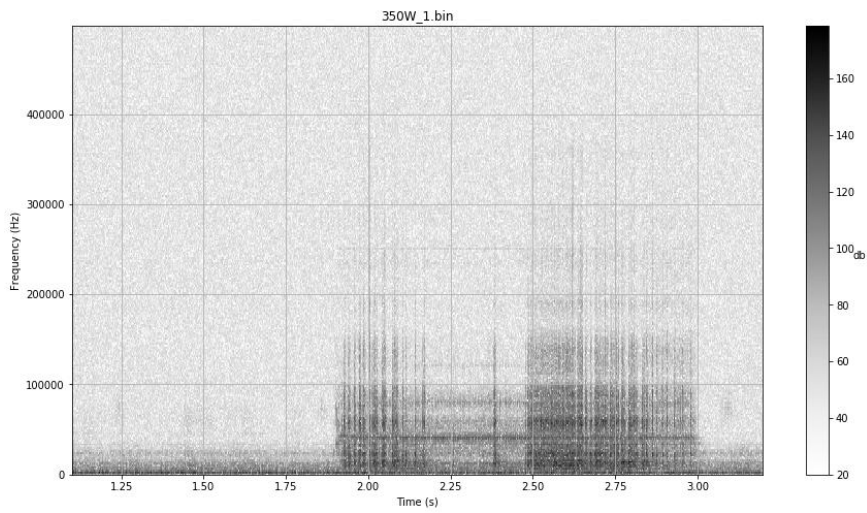


Figure 32: Spectrogram for the acoustic emission of a 350W laser process in the transition zone from heat conduction to keyhole/deep welding regime

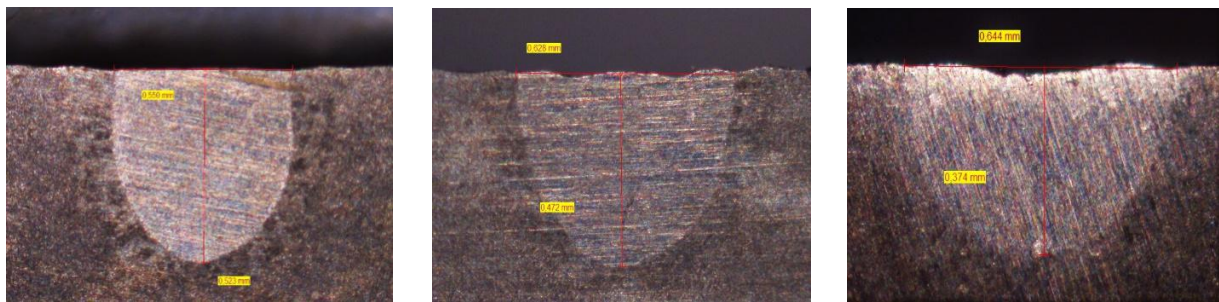


Figure 33: 3 weld seams from different cross sections of a workpiece treated in a 350W laser process

The most significant findings from this set of experiment is the correlation between the formation of a keyhole and the corresponding acoustic signature seen in the spectrograms. In the 3 sets of graphics above, it is important to observe the shape of the weld seam and the 'spikes' in the spectrogram. Aspect ratio is the term commonly used to qualify the shape of a weld seam, it is the ratio of the width of the weld seam to its depth. A flattened semicircle with low aspect ratio is the defining shape of a weld seam in the heat conduction regime, as seen in Figure 29. A consistent, deep and narrow weld seam with high aspect ratio is the defining shape of a keyhole weld seam, as seen in Figures 31. Comparing Figure 28 and 30, it is evident that the spectrograms differ in the presence and absence of higher frequency signatures. Given that both the 280W and 450W welding processes give off broadband sounds, the 450W process, in which the keyhole/deep welding regime is the dominant mechanism, emit much more intense and broader band sound. For the 280W process, there is negligible contribution from frequencies higher than 150 kHz, whereas for the 450W process, there is noticeable contribution from frequencies between 150 kHz to 400 kHz.

However from Figure 32 and 33 (and results from other adjacent power levels), it is observed that the shapes of the weld seam cross-sections cannot be conclusively classified into either of the groups described above, and so is the corresponding acoustic emission in the frequency domain. The transitions between the keyhole regime spectral signatures and heat conduction regime spectral signatures are abrupt instead of gradual. The welding laser was operating in continuous mode around the circumference of the cylindrical workpiece but the cross sections of the weld seams suggest that the effect on the workpiece may not be homogeneous at every point during the process.

Given the above results, further investigation into using the optical microphone as an instrument to monitor the presence of keyhole formation and sustenance during a welding process can be recommended. It has the potential to become a key component for non-destructive testing and monitoring during production, or be used in process development to determine the threshold for deep penetration welding without the necessity of preparing cross sections. A possible modification to the post-experiment analysis done in this case could be to increase the time resolution of the spectrogram by decreasing the size of the sliding window, in order to better pinpoint any moments of irregularity. There may be room for reduction in frequency resolution yet still preserving the distinguishing feature that separates a keyhole from the lack of one. An automated script could then check for any major discrepancies in the amplitude of the higher frequency bands.

A further showcase of the 'spikes' in the spectrograms can be found in appendix F.

5. Summary and Conclusion

The series of experiments has shown that the XARION Eta250 optical microphone along with the Optimizer4D system is able to provide an option for non-destructive monitoring of laser processes including ablation and welding and automated calibration of the laser focus spot. For ablation using the ultrashort pulse laser machine, the frequency of the laser pulses is evident and clearly captured by the microphone. The root-mean-square (RMS) value of the time signal of an ablation process correlates to the distance (in the z-axis) of the focal plane from the point with the smallest beam diameter. There could be a correlation between the power spectral density (PSD) and the z-coordinate offset too. For welding, there is a correlation between the power of the laser and the frequency of broader-band and more intense 'spikes' in the spectrogram.

The XARION optical microphone, as a measurement instrument during laser processes, has proven to be of good value. It can serve as a stable supplement with great potential and flexibility. The acoustic emission from these processes contain characteristics that correlates to the process parameters investigated. Further experimentation involving better optimized procedure (such as a synchronized trigger signal from the laser machine to the microphone) can be considered to confirm and more precisely qualify the correlations identified.

6. Acknowledgement

I would like to thank my supervisors Dr. Sven Döring and Professor Dr. Markus Pfeil for their continuous support and guidance throughout the entire duration of preparing this thesis. As my supervisor in the company and department, Dr. Döring has provided close mentorship with regards to the planning and execution of the content of this thesis. I would also like to thank all members and staff of the Technical Functions 1 department (TEF 1) of Robert Bosch GmbH (Bamberg Plant 4) for the pleasant working experience and all help afforded during my contract.

7. Appendix

Appendix A

The intensity of a Gaussian beam at any point on the focal plane (at the beam waist) is given as

$$I(r) = I_0 e^{-\frac{8r^2}{d_f^2}} \quad (i)$$

In which,

- I_0 is the peak laser intensity
- r is the radial distance from the center of the focal plane
- d_f is the diameter of the laser beam, determine by the radial distance at which the intensity is at $1/e^2$ of the peak intensity

Appendix B

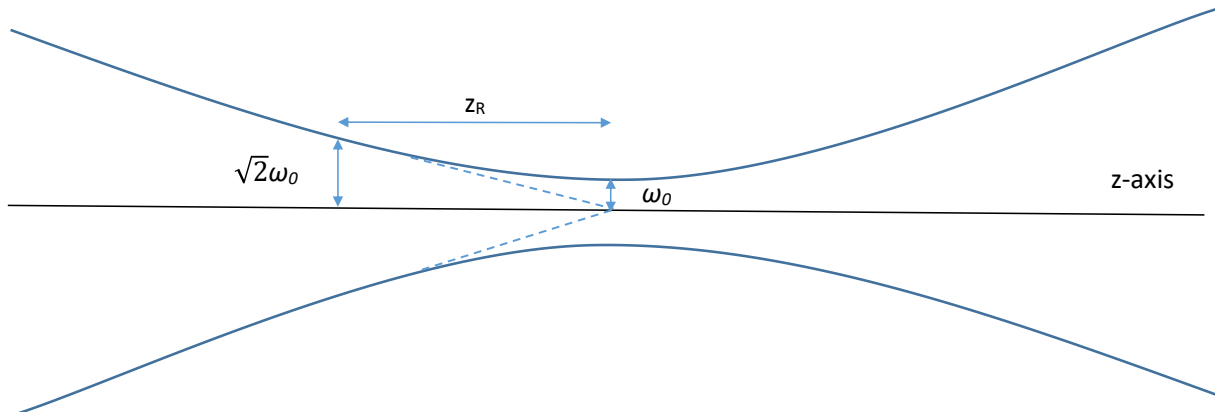


Figure 34: Illustration of a Gaussian beam, symmetrical about the z-axis. ω_0 is the beam waist, z_R is a quantity known as the Rayleigh length

The calculation of the optimum focus spot (smallest beam diameter), d_f , along the z-axis is given by

$$d_f = 2\omega_0 = \frac{4\lambda}{\pi} \frac{f}{d_{in}} \cdot M^2 \quad (\text{ii})$$

In which^[7]

- λ is the wavelength of the laser beam
- f is the focal length of the lens
- d_{in} is the input diameter of the beam just before passing through the focusing lens
- M^2 is the beam propagation factor, a quantity describing the variation of the beam from an ideal Gaussian beam

Appendix C

Fourier transformation is a mathematical process that deconstructs a time signal into its respective constituent frequency components, or in other words, indicating sinusoidal signals of all necessary frequencies for superposition to achieve the time signal in question. It is given by the formula below

$$X(\omega) = \int_{-\infty}^{\infty} x(t)e^{-j\omega t} dt \quad (\text{iii})$$

In which

- $X(\omega)$ is the amplitude of the frequency domain, $x(t)$ is the signal in the time domain
- ω is angular frequency
- t is time
- j is the imaginary number $\sqrt{-1}$

Once transformed, all time domain information exchanged for frequency domain information, all frequency components have their respective amplitude contributions. To visualize the frequency domain information over time for a signal, a technique known as Short-Time Fourier Transform (STFT) is used. It involves executing Fast Fourier transform (FFT, an algorithm capable of speeding up a Fourier transformation calculation) in a sliding window across the time axis with a fixed time width, from the start of the time signal to the end. For every single window, a spectrum is obtained, denoting the frequency components for the window of time. The spectra obtained from every instance of the sliding window is compiled to give a spectrogram (usually with frequency against time axes and another means of communicating amplitude). The discrete version of STFT is given by the formula below:

$$X(m, \omega) = \sum_{n=-\infty}^{\infty} x[n]w[n-m]e^{-j\omega n} \quad (\text{iv})$$

In which

- $x[n]$ is the discrete-time signal as a function of n
- $w[m]$ is a window function, which is non-zero only for a short time period

Each iteration in the summation computes a Fourier transform of $x[n]*w[n-m]$ at time step m to give the frequency information for that time step. As m changes (slides across the time axis), time-varying frequency information is revealed. It is important to note that the time resolution and the frequency resolution of a spectrogram produced by the STFT are inversely related. Any resolution gained in either domain will necessarily mean a loss in the other. The transformations in this thesis give 500 frequency bins of 2kHz bandwidth each.

Appendix D

Denoising of the spectrogram was done with the following steps:

1. Read in a signal of background noise when the laser machine is not in operation
2. Obtain the spectrogram of the noise signal by doing STFT
3. Calculate a mean of the amplitude of each frequency bin across the whole time axis to obtain a single column of amplitudes
4. Calculate the spectrogram of each process signal
5. For every process signal spectrogram, compare each frequency bin of every specific time slice with the corresponding frequency bin of mean noise amplitude obtained in step 3. If the amplitude of the frequency bin from the process signal is not at least 10 times greater than the amplitude in the noise counterpart, then the former is reduced to a fixed value of 1 ($\log 1$ gives 0 which is convenient as a standardized minimum value in the spectrogram); otherwise a subtraction is performed to remove the noise contribution.
6. The denoised signal is then plotted.

The justification for looking at amplitude 10 times greater than the noise counterpart is that within the same magnitude, the contribution from the process is difficult to ascertain. In other words, definitive contribution from the process signal will result in amplitude values several magnitudes higher, as evident in the spectrograms with a logarithmic scale in decibels.

Appendix E

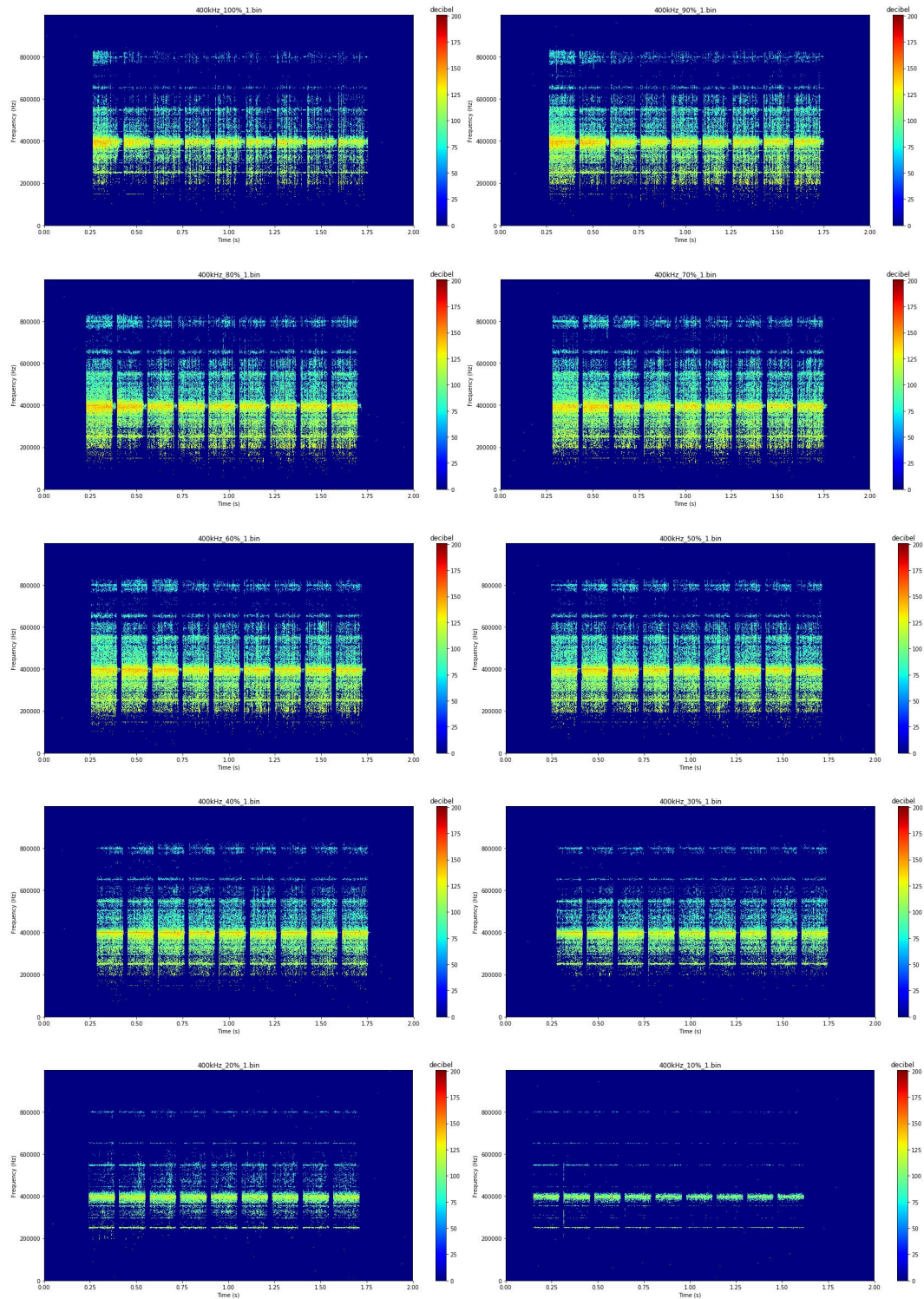


Figure 35: From left to right, then top row to bottom row: Spectrograms from experiment set 1, 400kHz ultrashort pulse laser at 100% to 10% laser power, 10% steps in between

Appendix F

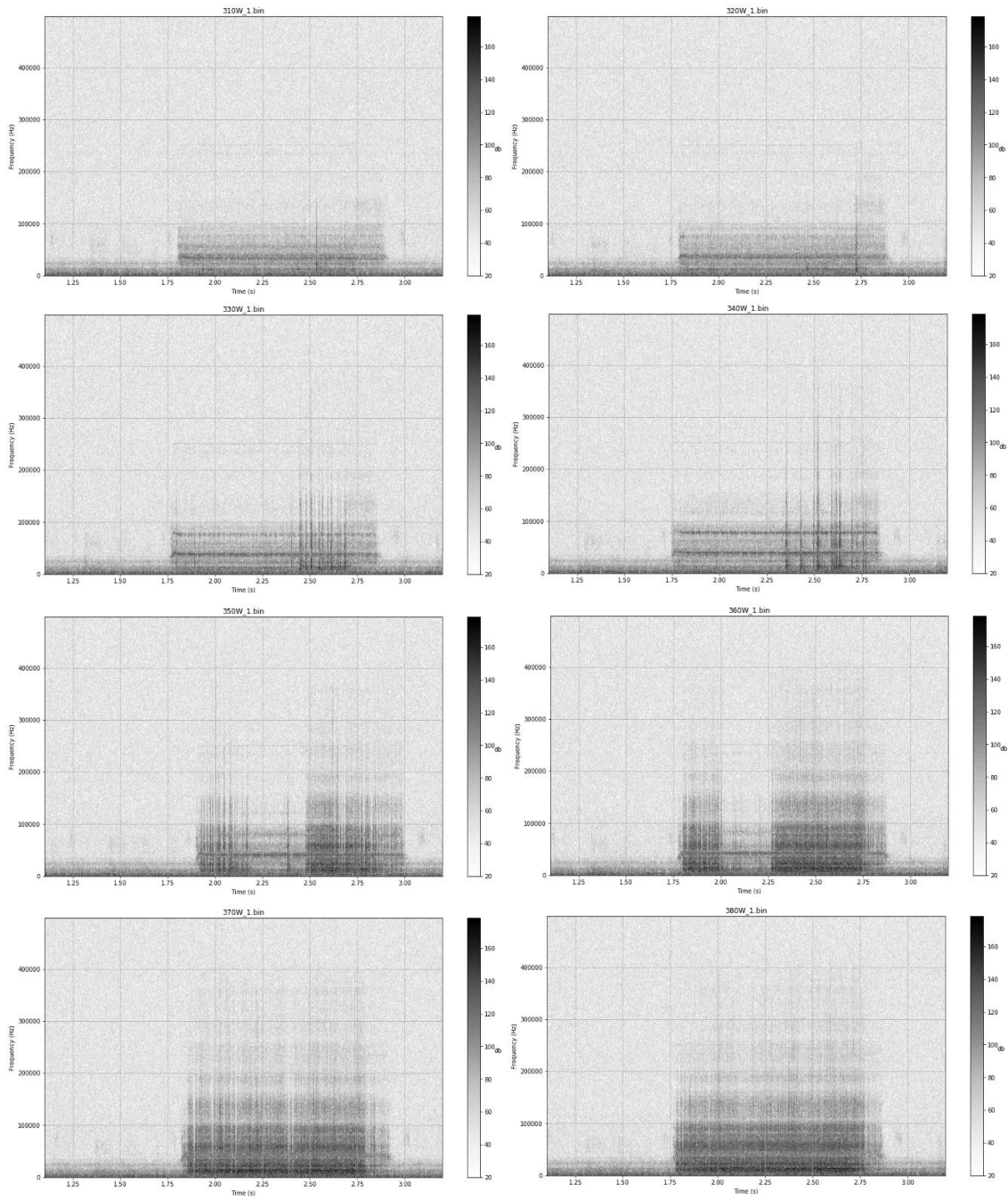


Figure 36: From left to right, top row to bottom, the spectrograms from experiment set 3, welding with laser power from 310W to 380W, with 10W step in between.

8. References

- [¹] Kacaras, A., Bächle, M., Schwabe, M., Zanger, F., León, F. and Schulze, V. (2019). Acoustic emission-based characterization of focal position during ultra-short pulse laser ablation. 52nd CIRP Conference on Manufacturing Systems.
- [²] Schulze, V. and Weber, P. (2010). Precise ablation milling with ultrashort pulsed Nd:YAG lasers by optical and acoustical process control. In: *SPIE LASE*. [online] SPIE. Available at: <https://www.spiedigitallibrary.org/conference-proceedings-of-spie/7585/75850J/Precise-ablation-milling-with-ultrashort-pulsed-Nd-YAG-lasers-by/10.1117/12.841616.full?tab=ArticleLink>.
- [³] Shelyagin, V., Zaitsev, I., Bernatskyi, A., Sydorets, V., Dubko, A. and Bondarenko, O. (2018). Contactless monitoring of welding processes with computer processing of acoustic emission signals. *2018 14th International Conference on Advanced Trends in Radioelectronics, Telecommunications and Computer Engineering (TCSET)*.
- [⁴] Hecht, E. (2017). *Optics*, Global Edition. 5th ed. Pearson Education Limited
- [⁵] Born, M. and Wolf, E. (1985). *Principles of optics*. 6th ed. Oxford, New York: Pergamon Press.
- [⁶] Rohringer, W., Heine, T., Sommerhuber, R., Lehmann, N. and Fischer, B. (2018). Optical Microphone as Laser-Ultrasound Detector. DAGA 2018 München. p.961.
- [⁷] von der Linde, D. and Sokolowski-Tinten, K. (2000). The physical mechanisms of short-pulse laser ablation. *Applied Surface Science*, 154-155, pp.1-10.
- [⁸] Steen, W. and Mazumder, J. (2010). *Laser material processing*. 4th ed. London: Springer.